(Finite) statistical size effects on compressive strength

Jérôme Weiss[a,1], Lucas Girard[b], Florent Gimbert[c,d], David Amitrano[d], and Damien Vandembroucq[e]

[a]Laboratoire de Glaciologie et Géophysique de l'Environnement, Centre National de la Recherche Scientifique (CNRS)/Université J. Fourier, 38402 St. Martin d'Hères Cedex, France; [b]Laboratoire des sciences cryosphériques, Institut d'ingénierie de l'environnement, Faculté de l'Environnement Naturel, Architectural et Construit, Ecole Polytechnique Fédérale de Lausanne, 1015 Lausanne, Switzerland; [c]Division of Geological and Planetary Sciences, California Institute of Technology, Pasadena, CA 91125; [d]Institut des Sciences de la Terre, CNRS/Université J. Fourier, 38041 Grenoble Cedex 9, France; and [e]Laboratoire Physique et Mécanique des Milieux Hétérogènes, Unité Mixte de Recherche 7636, CNRS/Ecole Supérieure de Physique et de Chimie Industrielles/Université Paris 6 Université Pierre et Marie Curie/Université Paris 7 Diderot, 75231 Paris Cedex 05, France

The larger structures are, the lower their mechanical strength. Already discussed by Leonardo da Vinci and Edmé Mariotte several centuries ago, size effects on strength remain of crucial importance in modern engineering for the elaboration of safety regulations in structural design or the extrapolation of laboratory results to geophysical field scales. Under tensile loading, statistical size effects are traditionally modeled with a weakest-link approach. One of its prominent results is a prediction of vanishing strength at large scales that can be quantified in the framework of extreme value statistics. Despite a frequent use outside its range of validity, this approach remains the dominant tool in the field of statistical size effects. Here we focus on compressive failure, which concerns a wide range of geophysical and geotechnical situations. We show on historical and recent experimental data that weakest-link predictions are not obeyed. In particular, the mechanical strength saturates at a nonzero value toward large scales. Accounting explicitly for the elastic interactions between defects during the damage process, we build a formal analogy of compressive failure with the depinning transition of an elastic manifold. This critical transition interpretation naturally entails finite-size scaling laws for the mean strength and its associated variability. Theoretical predictions are in remarkable agreement with measurements reported for various materials such as rocks, ice, coal, or concrete. This formalism, which can also be extended to the flowing instability of granular media under multiaxial compression, has important practical consequences for future design rules.

Owing to its importance for structural design (1), the elaboration of safety regulations (2), or the extrapolation of laboratory results to geophysical field scales (3), the size effects on strength of materials are one of the oldest problems in engineering, already discussed by Leonardo da Vinci and Edmé Mariotte (4) several centuries ago, but still an active field of research (5, 6). As early as 1686, Mariotte (4) qualitatively introduced the weakest-link concept to account for size effects on mechanical strength, a phenomenon evidenced by Leonardo da Vinci almost two centuries earlier. This idea, which states that the larger the system considered is, the larger the probability to find a particularly faulty place that will be at the origin of global failure, was formalized much later by Weibull (7). Considering a chain of elementary independent links, the failure of the chain is obtained as soon as one link happens to break. By virtue of the independence between the potential breaking events, the survival probability of a chain of N links is obtained by the simple multiplication of the N elementary probabilities. Depending on the properties of the latter, the global survival probability converges toward one of the three limit distributions identified by Weibull (7), Gumbel (8), and Fréchet (8), respectively. Together with Fisher and Tippett (9), these authors pioneered the field of extreme value statistics.

This purely statistical argument, undoubtedly valid in 1D, was extended by Weibull (7, 10) to account for the risk of failure of 3D samples or structures. Besides the hypothesis of independence, it thus requires an additional hypothesis of brittleness: The nucleation of any elementary crack at the microscopic scale from a preexisting flaw is assumed to immediately induce the failure at the macroscale. More specifically, following linear elastic fracture mechanics (LEFM) stating that crack initiation from a flaw of size s occurs at a stress $\sigma_c \sim s^{-1/2}$, one gets a probability of failure of a system of size L under an applied stress σ, $P_F(\sigma, L)$, that depends on the distribution of preexisting defect sizes. Assuming a power law tail for this distribution, Weibull statistics are expected(7), $P_F(\sigma, L) = 1 - \exp(-(L/L_0)^d (\sigma/\sigma_u)^m)$, whereas Gumbel statistics are expected for any distribution of defect sizes whose the tail falls faster than that of a power law (8, 11, 12), $P_F(\sigma, L) = 1 - \exp(-(L/L_0)^d \exp(\sigma/\sigma_u))$, where m is the so-called Weibull's modulus, d is the topological dimension, and L_0 and σ_u are normalizing constants. For Weibull statistics, the mean strength σ_f and the associated SD $\delta(\sigma_f)$ then scale with sample size L as $\sigma_f(L) \sim \delta(\sigma_f)(L) \sim L^{-d/m}$. This approach has been successfully applied to the statistics of brittle failure strength under tension (7, 13), with m in the range 6–30 (14). It implies a vanishing strength for $L \to +\infty$, although this decrease can be rather shallow, owing to the large values of m often reported.

Although relying on strong hypotheses, this weakest-link statistical approach was almost systematically invoked until the 1970s to account for size effects on strength whatever the material and/or the loading conditions. However, as shown by Bazant (1, 5), in many situations the hypothesis of brittleness is not obeyed. This is in particular the case when the size of the fracture process zone (FPZ) becomes nonnegligible with respect to the system size. In this so-called quasi-brittle case, an energetic, nonstatistical size effect applies (15), which has been shown to account for a large variety of situations (5). Toward large scales, i.e., $L \to +\infty$, the FPZ becomes negligible compared with L, and the hypothesis of brittleness should therefore be recovered and statistical size effects should dominate. Statistical numerical models of fracture of heterogeneous media also revealed deviations from the extreme value statistics predictions (16) but, as stated by Alava et al. (ref. 11, p. 9),

Significance

Large structures generally fail under stresses significantly lower than those of small ones. This is the size effect on strength, one of the oldest problems of engineering, already discussed by Leonardo da Vinci and Edmé Mariotte centuries ago. One classical explanation is the weakest-link hypothesis: The larger the "chain" is, the larger the probability to find a weak link whose breaking will set the failure of the whole chain. We show, however, that it is irrelevant in the case of compressive loading, a situation particularly crucial for, e.g., geotechnical problems. Interpreting compressive failure as a critical transition between an "intact" and a "failed" state, we quantitatively explain the size effects on compressive strength of materials such as concrete, rocks, coal, ice, or granular materials.

ENGINEERING

"the role of damage accumulation for fracture size effects in unnotched samples still remains unclear." As shown below, compressive failure results from such progressive damage accumulation.

In what follows, we do not consider (deterministic) energetic size effects and explore a situation, compressive failure, where both the hypotheses of brittleness (in the sense given above) and independence are not fulfilled, up to very large scales. Relaxing these initial hypotheses of the weakest-link theory, our statistical physics approach remains statistical by nature and relies on the interplay between internal disorder and stress redistributions. It is based on a mapping of brittle compressive failure onto the critical depinning transition of an elastic manifold, a class of models widely used in nonequilibrium statistical physics characterized by a dynamic phase transition (17). This approach does not consider a sample's shape effects (18), only statistical size effects. The critical scaling laws associated to this phase transition naturally predict a saturation of the compressive strength at a large scale and are in remarkable agreement with measurements reported for various materials such as rocks, ice, coal, or concrete.

Compressive Failure Cannot Be Captured by a Weakest-Link Approach

Compressive loadings are particularly relevant in rock mechanics and geophysical situations (19) as the result, e.g., of lithostatic pressure and consequently for geotechnical problems (e.g., ref. 18). Brittle compressive failure is a complex process, as the local tensile stresses at crack tips are counteracted by the far-field compressive stresses. Consequently, Griffith-like energy balance arguments, or related tools such as fracture toughness, cannot be developed to describe the instability leading to terminal failure, thus making the weakest-link approach inoperative. Instead, brittle compressive failure involves an initiation phase, elastic interactions, and stress redistributions, as well as frictional sliding along rough surfaces. In what follows, we mean by brittle failure a situation where microscopic ductile deformation processes such as creep or dislocation motion play a negligible role (20). During the initiation phase, secondary cracks nucleate from the local tensile stresses generated by the frictional sliding along preexisting defects such as grain boundaries, small joints, or microcracks (21, 22). The propagation of these mode I secondary cracks is, however, rapidly stopped by the far-field compression. Instead, such nucleation events locally soften the material (23, 24) and thus cause a redistribution of elastic stresses, which in turn can trigger other microcrackings. Then, in the course toward failure, the interaction and linking of secondary cracks are considered to be at the onset of shear fault formation, from which the macroscopic instability is thought to result (22, 25). This process is characterized by a progressive localization of damage and deformation along a fault (26).

The above description shows that all of the assumptions of the weakest-link theory are inappropriate in the case of compressive failure. Summarizing experimental field and laboratory data obtained for 50 y, it is thus not surprising that their weakest-link predictions are poorly obeyed. When the compressive strength of brittle materials has been measured from laboratory tests over a limited scale range (generally between $\sim 10^{-2}$ m and $\sim 10^{-1}$ m), either nonsignificant (27, 28) or limited (29, 30) size effects on σ_f were observed, whereas, when reported, the associated variance seemed to increase toward small scales (27). Consequently, these results do not fully constrain empirical or theoretical size effect formulations. Some studies were performed instead several decades ago over a much larger scale range ($\sim 10^{-2}$ m to a few meters), combining laboratory and in situ tests (18, 31–33). All of them reported a significant scale dependence of σ_f at small scales, tentatively and empirically fitted as a power law decrease (18) $\sigma_f(L) \sim L^{-\beta}$, but also a nonzero asymptotic strength at large (>1 m) scales, not explained by the weakest-link approach. So far, there is no clear explanation for this nonvanishing compressive strength. Instead, empirical formulations of size effects on compressive strength of brittle materials (3, 18, 34) generally ignore such asymptotic behavior. Following observations at small

scales, they all share a common power law scaling $\sigma_f \sim L^{-\beta}$, with β varying from very small values (29) (i.e., almost no size effect) to the LEFM scaling $\beta = 1/2$. The weakest-link concept has been sometimes put forth to explain this scaling for small β values (29), although it is clear from the above that this approach is irrelevant in the case of compressive failure. On the other hand, a (deterministic) energy analysis of compression failure based on physical (micromechanical) considerations has been proposed (1, 35). In agreement with the scenario described above, it considers that the nucleation of microcracks roughly parallel to the principal compression axis forms a band whose mechanical instability, triggered by the buckling of the microslabs separating the microcracks, leads to failure. However, the microcracks, and therefore the associated band, are assumed to nucleate suddenly, just preceding macrofailure; i.e., this approach does not consider the progressive route toward the failure, characterized by elastic interactions between cracks and progressive damage localization. In other words, the transition to failure is considered a "first-order" transition. This, in addition to an assumed constant scaling between the band length and the size of the system, gives a vanishing strength toward large scales with an asymptotic scaling $\sigma_f \sim L^{-2/5}$, i.e., slightly shallower than the LEFM scaling. Consequently, the observed nonvanishing strength σ_∞ is not explained. In addition, this deterministic approach cannot, by nature, account for a size dependence of the variability of strength. We propose instead to consider compressive failure as a critical transition and develop a mapping onto the depinning transition that allows accounting for the interplay between local disorder and long-ranged elastic interactions, leading to a statistical finite size effect.

Compressive Failure as a Critical Depinning Transition

The modeling of the mechanical behavior of heterogeneous materials induced in recent years an intense research activity. In the early 1990s the idea emerged that nonlinear processes such as fracture, plasticity, and damage could be discussed as critical phenomena (36). In the context of damage, a paradigmatic example of this approach is given by the fiber bundle model (37). However, the scope of this model as well as its variants (38) are restricted to the catastrophic failure occurring under tensile conditions, i.e., the transition from an initiation stage to a propagating stage triggered by the development of a critical nucleus. In contrast, our interest here is the study of progressive damage under compressive conditions. To our knowledge the first attempt of a description of compressive damage as a critical phenomenon is due to Toussaint and Pride (39). They developed a statistical mechanics formalism based on ensemble averages obtained over the rock seen as a collection of disordered mesovolumes. A specific Hamiltonian (40) that accounted for the interaction between cracks and the traditional tools of equilibrium statistical mechanics (partition function, maximum of entropy) were used to characterize the localization transition associated with the failure of the material.

We here follow a different route. We proposed recently a numerical progressive damage model whose results are consistent with an interpretation of brittle compressive failure as critical phase transition (41, 42). This finite-element model (41) considered a continuous elastic material with progressive local damage: The elastic modulus of an element decreases each time the stress state on that element exceeds a given threshold defined by a Coulomb criterion. This elastic softening simulates an increase in microcrack density at the element scale (23, 24). Disorder was introduced on the local stress threshold. As the result of elastic interactions, the stress redistribution following a damage event can trigger an avalanche of damage. We showed (41, 42) (*i*) that the size of the largest damage cluster and that of the largest damage avalanche diverge at peak load, which just precedes failure, and (*ii*) the divergence of a correlation length ξ at failure, $\xi \sim \Delta^{-1/\nu}$, where $\Delta = (\epsilon_{mf} - \epsilon_m)/\epsilon_{mf}$ (respectively $\Delta = (\sigma_f - \sigma)/\sigma_f$) is the control parameter for strain- (respectively stress)-driven simulations, ϵ_m is the applied macroscopic strain, ϵ_{mf} is the corresponding value at peak stress σ_f (failure), and $\nu = 1.0 \pm 0.1$ is the correlation length exponent.

Here, in the spirit of a recent model of amorphous plasticity (43), we formalize this interpretation of compressive failure as a critical transition through a mapping onto a depinning model, a class of models that exhibit out-of-equilibrium phase transition. The damaging process is described as the motion of a d-dimensional elastic manifold with long-range interactions through a random field of obstacles within a space of dimension $d + 1$. In our case, the macroscopic stress plays the role of the driving force and a local damage event corresponds to the depinning from an obstacle, with elastic redistributions in both cases. Damage is represented by a scalar field $D(\mathbf{r})$ at a mesoscopic scale λ, which typically corresponds to the correlation length of the structural disorder of the material, and it occurs whenever the stress state $\boldsymbol{\sigma}$ reaches the boundary of an elastic domain defined by the Coulomb criterion, $|\tau| + \mu\sigma_N = \tau_C$. This criterion is of wide applicability for brittle materials under compressive stress states to define the onset of damage (19, 44). τ and σ_N are, respectively, the shear and normal stress (sign convention positive in tension) over a plane maximizing the Coulomb stress $|\tau| + \mu\sigma_N$, and $\mu = \tan(\varphi)$ is an internal friction coefficient (φ is the so-called angle of internal friction). The heterogeneous nature of the material, i.e., the disorder, is accounted for by a statistical variability of the cohesion τ_C, $\delta\tau_C$.

A crucial feature is the nonindependence of the local damaging events occurring in the material. Any local event is characterized by a local decrease of the elastic modulus that occurs in a small region surrounded by the remainder of the material. The latter can be seen as an elastic matrix and its reaction induces an elastic stress field all over the material. We started from the classical inhomogeneity problem of Eshelby (45, 46) to calculate the stress field induced by a damaged inclusion. Because the damaged material is elastically disordered, the internal stress cannot be obtained by a simple superposition of the contributions of isolated inclusions. To partly account for interactions between inclusions, we develop a two-step strategy to compute the internal stress (*SI Text*). The damage field is first used to obtain a self-consistent estimate of the average, macroscopic elastic behavior, $\overline{E}$. This effective value, which partly accounts for interactions between inclusions, is then used to obtain a fluctuating damage field, defined from the contrast between the actual elastic moduli at microscale and $\overline{E}$. The internal stress is finally obtained from the sum of the elastic contributions of the associated effective inclusions. The interplay between local disorder and elasticity is the basis for depinning models, which have proved successful in recent years to describe physical and mechanical phenomena as various as the advance or retreat of a triple contact line on a disordered substrate (47–49), the motion of a magnetic wall in a thin film (50), the propagation of a crack front in a heterogeneous material (51–54), etc. The full derivation of our problem is given in *SI Text*. It allows a complete mapping onto a depinning model, with the following equation of evolution of the damage field,

$$\mathsf{M}\frac{\partial D}{\partial t}(\mathbf{r}) = \mathcal{R}\left[\sigma_s^{\text{ext}} + \sigma_s^{\text{el}}(\{D\}, \overline{E}(\{D\}), \mathbf{r}/\lambda) - 2\cos(\varphi)\tau_C(\mathbf{r}, D)\right], \quad [1]$$

where $\mathcal{R}$ denotes the positive part, M is a mobility coefficient, and λ is the characteristic length scale of the microstructural disorder. In the language of depinning models, we identify σ_s^{ext} as the external forcing term, σ_s^{el} as the elastic contribution induced by the damage field D, via the knowledge of the damage-dependent effective modulus $\overline{E}$, and τ_C is the disorder.

This formal mapping enables us to apply to progressive damage the various analytical and numerical results obtained in the framework of the depinning transition. In the "thermodynamic" limit, i.e., for a system of infinite size, a well-defined critical threshold σ_{th} separates the static phase (limited damage) from the dynamic one (failure). For our problem, this is the expression of a nonvanishing asymptotic strength, $\sigma_\infty > 0$. In the case of samples of finite size, fluctuations of the measured threshold σ_f are expected in the vicinity of σ_{th}. We thus expect, as for the threshold force of the depinning

transition (6, 55), a finite-size scaling for the compressive strength σ_f of the form

$$\delta(\sigma_f)(L) = A L^{-1/\nu_{\text{FS}}}, \quad \text{or} \quad \frac{\delta(\sigma_f)(L)}{\sigma_\infty} = \left(\frac{L}{L_A}\right)^{-1/\nu_{\text{FS}}} \quad [2]$$

$$\sigma_f(L) = B L^{-1/\nu_{\text{FS}}} + \sigma_\infty, \quad \text{or} \quad \frac{\sigma_f(L)}{\sigma_\infty} = \left(\frac{L}{L_B}\right)^{-1/\nu_{\text{FS}}} + 1, \quad [3]$$

where ν_{FS} is the finite-size exponent and σ_∞ is a nonvanishing asymptotic value of the strength for $L \to +\infty$. A, B (in $Pa.m^{1/\nu_{\text{FS}}}$), $L_A = (A/\sigma_\infty)^{\nu_{\text{FS}}}$, and $L_B = (B/\sigma_\infty)^{\nu_{\text{FS}}}$ (in meters) are constants. These length scales define the scales below which, respectively, the fluctuations and the finite-size corrections become important compared with the asymptotic strength σ_∞. We expect these to scale as $L_{A,B} \sim \lambda(\delta\tau_c/\tau_c)^{\nu_{\text{FS}}}$, where $\delta\tau_c/\tau_c$ represents the associated variability on the local cohesive strength (*SI Text*). This implies that in the case of weak disorder L_A and L_B will be of the order of λ (e.g., grain size, aggregate size, etc.), but might be significantly larger in the case of strong disorder when, e.g., cracks or joints widely distributed in size are initially present in the material. The classical assumption (55) is $\nu = \nu_{\text{FS}}$, whereas the mean-field prediction (56) is $\nu = 1$. Eq. **2** expresses the variability on strength intrinsically related to the failure process, to which experimental sources of variability should be added. Toward very small scales, $L \ll \lambda$, the proposed scaling (Eqs. **2** and **3**) necessarily breaks down when σ_f approaches the material strength limit (1).

Application to Experimental Data in Cohesive Materials

In full qualitative agreement with experimental data (see above), this finite-size scaling implies an apparent power law decay of the mean strength at small sizes, a nonvanishing strength for $L \to +\infty$, and an increasing variability toward small sizes. Relation [2] is hardly testable from experimental data, as $\delta(\sigma_f)$ values, when reported, are based on a limited number of independent tests and include experiment-related scatter. For studies including field tests at the meter scale (18, 31–33) and assuming that the asymptotic strength σ_∞ was reached at the largest scale, we fitted the data with relation [3]. The agreement is remarkable, with the best-fit ν_{FS} value ranging from 0.8 to 1.05 (Fig. 1), i.e., close to the mean-field prediction, $\nu = 1$. The corresponding length scales L_B range from ~20 cm to 40 cm, a possible sign of relatively strong disorder (joints, microcracks) in these natural rock samples. For studies based only on laboratory tests, either (*i*) no significant size effect on strength is reported, as for fresh-water granular ice (27), limestone (57), granite (57), or concrete (28) (this can be explained by a small L_B in Eq. **3** and/or an insufficient dataset to properly sample size effects), or (*ii*) the data can be well fitted by [3], assuming $\nu_{\text{FS}} = 1$, as shown in Fig. S1 for high-performance (HP) concrete (30) and marble (29). In the case of HP concrete, the scale L_B is close to the maximum size of the andesite aggregate (12 mm) (30). In agreement with our former expectation, in such initially unfractured materials, the microstructural scale (aggregate size, grain size, etc.) likely sets this L_B scale.

The confining pressure σ_3 increases the axial compressive strength σ_{1f} of rocks, ice, coal, or concrete (19, 28, 34, 58). Up to a confining ratio σ_3/σ_{1f} of about 30%, failure is brittle and occurs through microcrack initiation and interactions, followed by shear fault formation at the onset of macroscopic instability, as described above (58). This failure mode is sometimes called Coulombic faulting, reminiscent of the importance of solid friction in this case (44). Consequently, one expects our mapping to the depinning transition to hold in this case. The combination of the effects of size and of confining pressure on strength has been rarely studied, but the available data on coal (34) are well explained by Eq. **2** with $\nu_{\text{FS}} = 1$ and an increasing asymptotic strength σ_∞ with increasing confinement, as expected (Fig. 2). For these natural samples, the scale L_B is once again relatively large (several centimeters). It
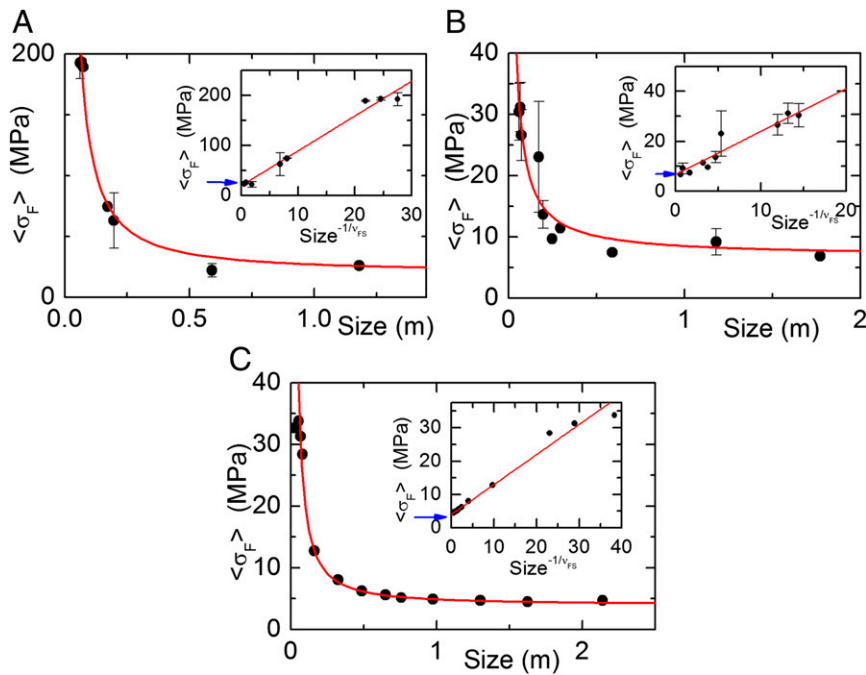
Fig. 1. Finite-size effect on uniaxial compressive strength (experimental data). (*A*) Granodiorite (31); (*B*) quartz diorite (31); (*C*) coal (32). Main graphs: mean compressive strength σ_f vs. size. Black circles: published experimental data, with associated SD (when reported). Red curve: fit by Eq. **3**, using $\sigma_\infty = 20$ MPa for granodiorite, 6.8 MPa for quartz diorite, and 4 MPa for coal. The best-fit ν_{FS} exponents are, respectively, 0.85, 1.05, and 0.8. The associated constants length scales L_B are, respectively, 0.41 m, 0.235 m, and 0.30 m. *Insets* show the same data and fits, in a σ_f vs. $L^{-1/\nu_{FS}}$ graph where Eq. **3** is a straight line and reveals the asymptotic strength σ_∞.

slightly decreases with increasing confinement, suggesting a secondary effect of confinement on the sensibility of L_B to the variability of the local strength, $\delta\tau_c/\tau_c$. For such multiaxial compression tests, the deviatoric stress $\sigma_1 - \sigma_3$ appears to be the most relevant variable. Thus, the strength has been defined as $\sigma_f = \sigma_{1f} - \sigma_3$. This choice for σ_f, instead of the axial strength σ_{1f}, obviously does not change the value of the exponent ν_{FS} or of the scale L_B. For confinements larger than ~30%, compressive failure is no more brittle, and another failure mode occurs, as mode I secondary crack nucleation is inhibited. This failure mode, called plastic faulting, involves thermal softening and an adiabatic shear instability (59). In this case, we no longer expect elastic interactions between microcracks to occur, i.e., our size effect formalism to hold. Indeed, it has been found that for large confining pressure, size effects on compressive strength disappear (60). This sets the range of applicability of our formalism.

Application to Granular Media

This mapping onto the depinning problem is likely not restricted to brittle cohesive materials. As described in ref. 43 and recalled in *SI Text*, it can be extended to the macroscopic plastic instability in amorphous media. The case of a cohesionless frictional granular medium compressed under confinement can be interpreted as an intermediate case between amorphous plasticity and compressive damage. Indeed, shear-induced local rearrangements of the granular structure lead to irreversible local strains but not to a systematic degradation of local stiffness. Compared with amorphous plasticity,

other complications are present, however, such as dilatancy. When compressed under confinement, these media exhibit a macroscopic flowing instability associated to strain localization (61), which sets the yield stress, i.e., the "strength." This instability can also be considered a critical transition (62). In this case, the disorder is topological, coming from the arrangement of particles.

From this analogy, we expect finite-size scaling (relations [**2**] and [**3**]) to ensue. However, to our knowledge, there is so far no experimental data over a significant range of scales to check this anticipation. We therefore simulated the mechanical behavior of frictional granular materials, using the molecular dynamics discrete element method (63). Two-dimensional granular assemblies made of a set of frictional circular grains were considered. The dynamic equations were solved for each of the grains, which interact via linear elastic laws and Coulomb friction when they are in contact (64). Neither cohesion between grains nor rolling resistance was considered. To build granular assemblies with strongly different initial (before loading) characteristics, in terms of coordination number and/or packing density, specific sample preparation procedures were used. Details on the discrete element model as well as on these procedures are given in *SI Text*. These granular assemblies were loaded under a multiaxial configuration, with the external axial stress σ_1 prescribed to impose a constant axial strain rate, whereas the radial stress σ_3, i.e., the confining pressure, was kept constant. The 2D sample sizes varied from 100 grains to ~45,000 grains.

Fig. 2. Finite-size effect on multiaxial compressive strength for coal (experimental data). These strength values have been recalculated using the generalized Hoek and Brown empirical formulation (equation 1 of ref. 34) and using the set of parameters found in table 3 of the same ref. 34, for confining pressure $\sigma_3 = 0$ MPa, 2 MPa, 5 MPa, and 9 MPa. (*A*) Mean compressive strength $\sigma_f = \sigma_{1f} - \sigma_3$ vs. size. For this multiaxial loading, the deviatoric stress has been considered here as the relevant variable. The corresponding fits from Eq. **3** of the main text, using $\nu_{FS} = 1$, are shown as lines. The best-fit asymptotic strengths σ_∞ are, respectively, 6.1 MPa, 16.6 MPa, 26.9 MPa, and 37.4

MPa for $\sigma_3 = 0$ MPa, 2 MPa, 5 MPa, and 9 MPa. The associated L_B values are, respectively, 27 cm, 12 cm, 9 cm, and 7.5 cm. (*B*) Same data and fits, in a σ_f vs. $L^{-1/\nu_{FS}}$ graph where Eq. **3** is a straight line and reveals the asymptotic strength σ_∞.
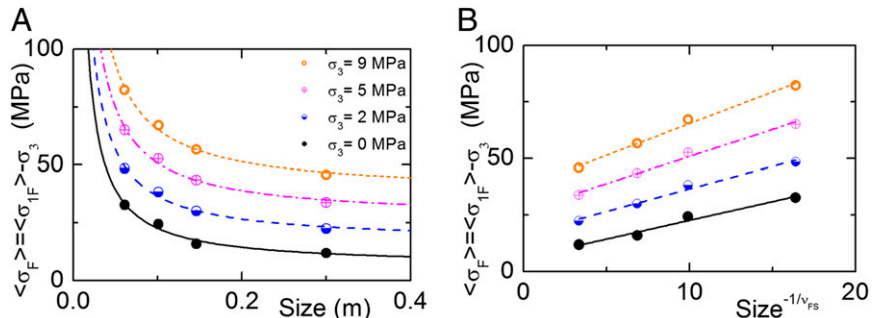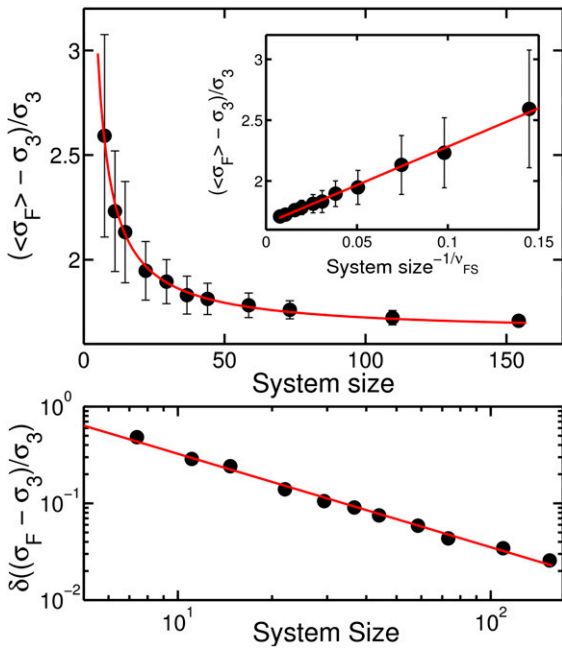
Fig. 3. Finite size effects for the discrete-element model of frictional granular media under multiaxial compression [low-coordinated (LC)1 samples; see SI Text for details about the model] and then normalized by the confining pressure σ_3. (*Upper*) Mean compressive strength $\sigma_f/\sigma_3 = (\sigma_{1f} - \sigma_3)/\sigma_3$; (*Lower*) associated SD vs. system size. System size has been defined as $\sqrt{N_g}$, where N_g is the number of grains of the model. Black circles: model results. Red curves: finite size scaling given by Eq. **3** for the mean strength and Eq. **2** for the SD, with $\nu_{FS} = 1.07$, $L_A = 1.68$, $L_B = 4.21$, and $\sigma_\infty = 1.65 \times \sigma_3$. The best-fit exponent ν_{FS} and scale L_A were obtained from the SD scaling (*Lower*), and the asymptotic strength σ_∞ and scale L_B were then obtained from the scaling of σ_f/σ_3 (*Upper*, *Inset*). *Inset* shows the same data and fits, in a σ_f/σ_3 vs. $L^{-1/\nu_{FS}}$ graph where Eq. **3** is a straight line and reveals the asymptotic strength σ_∞.

Whatever the initial characteristics of the assemblies, finite size scaling of compressive strength was observed, in full agreement with Eqs. **2** and **3** (Fig. 3), showing the generic nature of the concept proposed here. In agreement with our expectation, the scales L_A

and L_B were slightly larger than the average particle size and increased for less dense, less coordinated samples (Table S1).

Failure Strength Statistics

As noted in the Introduction, the weakest-link hypothesis leads to extreme value statistics for the probability of failure under an applied stress σ. As the weakest-link theory appears irrelevant for compressive failure, we do not expect such extreme statistics for the distribution of strength in this case. Published experimental data with a sufficient number of failure tests to analyze strength distributions are rare. Results obtained on ice indeed exclude extreme statistics, either Weibull or Gumbel, and argue instead for Gaussian statistics (Fig. 4). The same is true for the discrete-element modeling of frictional granular media (Fig. S2). We anticipate, from the criticality of the transition, the scaling form of the distribution $P(\sigma_f, L)$ of the fluctuations for a system of size L as $P(\sigma_f, L) = L^{\nu_{FS}} \Psi[(\sigma_{th} - \sigma_f)L^{\nu_{FS}}]$. Such a scaling form naturally leads to the scaling relations for the mean value σ_f (relation [3]) and the SD $\delta(\sigma_f)$ (relation [2]) of the compressive strength discussed above. However, the precise form of the statistical distribution Ψ is not prescribed by this simple scaling analysis. In particular, Ψ is not expected to obey the predictions of extreme value statistics whose hypotheses (absence of interactions) are not satisfied in the present problem. In recent results obtained in a similar framework [depinning model of amorphous plasticity (65)], Gaussian-like distributions were observed as well.

Combining Gaussian statistics with Eqs. **2** and **3** leads to the following expression for the probability of failure at scale L under a stress σ:

$$P_F(\sigma, L) = \frac{1}{2}\left[1 + \text{erf}\left(\frac{\sigma - \sigma_\infty\left(1 + (L/L_B)^{-1/\nu_{FS}}\right)}{\sqrt{2}\,\sigma_\infty(L/L_A)^{-1/\nu_{FS}}}\right)\right]. \quad [4]$$

Concluding Comments

This statistical physics interpretation of compressive failure of continuous and granular media has important practical consequences. First, when laboratory-scale (centimeter to decameter) studies show no significant size effect, one expects that laboratory strength values will give a good estimate of the asymptotic (field) strength. Extrapolation of laboratory-scale data to scales smaller than L_A or L_B will be more difficult, owing to the intrinsic variability at such scales. However, the mean-field estimate of the finite-size exponent, $\nu_{FS} = 1$, obtained from theoretical considerations, well
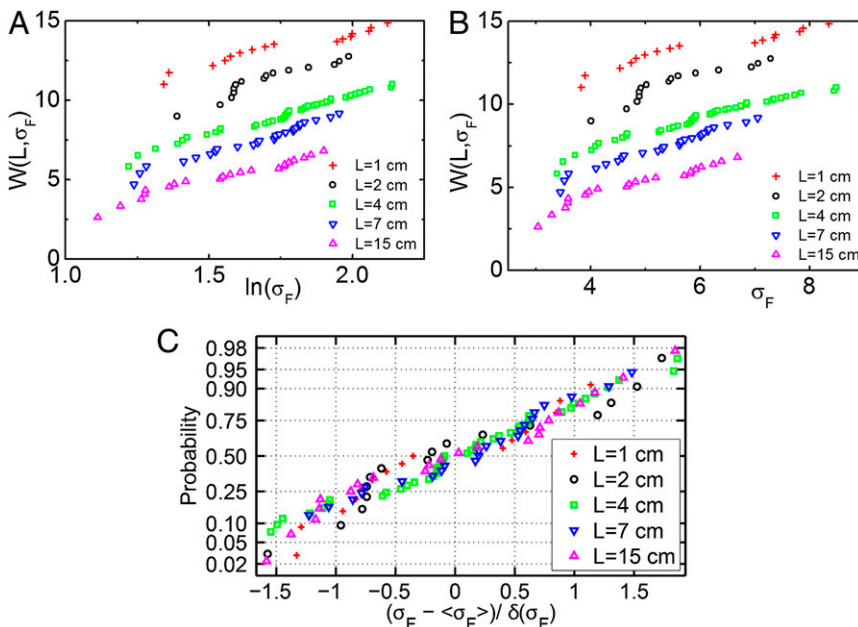

Fig. 4. Distribution of uniaxial compressive failure strength for fresh-water granular ice (grain size: ~1 mm), from ref. 27. (*A*) Weibull statistics, where $W(L, \sigma_f) = \ln(-\ln(1 - P_F(\sigma))/L^3)$ and $P_F(\sigma)$ is the (cumulative) probability of failure under an applied stress σ. Because data obtained for different sample sizes do not collapse onto a single straight line, compressive strengths do not follow Weibull statistics. (*B*) The same is true for Gumbel statistics. (*C*) Normal probability plot for the standard distributions. The collapse onto a single straight line, which corresponds to Eq. **4**, argues for Gaussian statistics.

describes the fluctuations and the associated finite-size corrections, whereas for initially unfractured materials, L_A and L_B are related to the characteristic microstructural scale (grain size, aggregate size, etc.). Therefore, owing to its predictive potential, we believe that the proposed scaling is a useful, simple to use guidance for future structural design rules or regulations (e.g., ref. 2).

Materials and Methods

The characteristics and the simulation settings of the discrete-element model of frictional granular media are given in SI Text, along with the formal derivation of the mapping of brittle compressive failure onto the depinning transition of an elastic manifold. All the experimental data analyzed here have been obtained from the literature.

1. Bazant ZP, Planas J (1998) *Fracture and Size Effect in Concrete and Other Quasibrittle Materials* (CRC, Boca Raton, FL).
2. European Committee for Standardization (2002) *Eurocode 2: Design of Concrete Structures - Part 1-1: General rules and rules for buildings*, EN 1995-1-1 (European Committee on Standardization).
3. Heuze FE (1980) Scale effects in the determination of rock mass strength and deformability. *Rock Mech* 12:167–192.
4. Mariotte E (1686) [*Traité du Mouvement des Eaux et des Autres Corps Fluides*] (Paris). French.
5. Bazant ZP (2004) Scaling theory for quasibrittle structural failure. *Proc Natl Acad Sci USA* 101(37):13400–13407.
6. Zapperi S (2012) Current challenges for statistical physics in fracture and plasticity. *Eur Phys J B* 85:329.
7. Weibull W (1939) A statistical theory of the strength of materials. *Proc R Swedish Acad Eng* Sci 151:1–45.
8. Gumbel EJ (1958) *Statistics of Extremes* (Columbia Univ Press, New York).
9. Fisher RA, Tippett LHC (1928) Limiting forms of the frequency distribution of the largest or smallest members of a sample. *Math Proc Camb Philos Soc* 24(2):180–190.
10. Weibull W (1951) A statistical distribution function of wide applicability. *J Appl Mech* 18:293–297.
11. Alava MJ, Nukala P, Zapperi S (2009) Size effects in statistical fracture. *J Phys D Appl Phys* 42(21):214012.
12. Sornette D (2000) *Critical Phenomena in Natural Sciences* (Springer, Berlin).
13. Beremin FM (1983) A local criterion for cleavage fracture of a nuclear pressure vessel steel. *Metallurgical Trans A* 14(11):2277–2287.
14. Miannay D (1998) *Fracture Mechanics* (Springer, Berlin).
15. Bazant ZP (1984) Size effect in blunt fracture - concrete, rock, metal. *J Eng Mech* 110(4):518–535.
16. Alava MJ, Nukala PKVV, Zapperi S (2006) Statistical models of fracture. *Adv Phys* 55(3–4):349–476.
17. Fisher DS (1998) Collective transport in random media: From superconductors to earthquakes. *Phys Rep* 301:113–150.
18. Hustrulid WA (1976) A review of coal pillar strength formulas. *Rock Mech* 8:115–145.
19. Jaeger JC, Cook NGW (1979) *Fundamentals of Rock Mechanics* (Chapman & Hall, London).
20. Schulson EM (2001) Brittle failure of ice. *Eng Fract Mech* 68(17–18):1839–1887.
21. Nemat-Nasser S, Horii H (1982) Compression-induced nonplanar crack extension with application to splitting, exfoliation, and rockburst. *J Geophys Res* 87:6805–6821.
22. Schulson EM, Iliescu D, Renshaw C (1999) On the initiation of shear faults during brittle compressive failure: A new mechanism. *J Geophys Res* 104:695–705.
23. Kachanov M (1994) Elastic solids with many cracks and related problems. *Adv Appl Mech* 30:259–445.
24. Cox SJD, Meredith PG (1993) Microcrack formation and material softening in rock measured by monitoring acoustic emissions. *Int J Rock Mech Min Sci Geomech Abstr* 30(1):11–24.
25. Katz O, Reches Z (2004) Microfracturing, damage, and failure of brittle granites. *J Geophys Res Solid Earth* 109:B01206.
26. Lockner DA, Byerlee JD, Kuksenko V, Ponomarev A, Sidorin A (1991) Quasi-static fault growth and shear fracture energy in granite. *Nature* 350(6313):39–42.
27. Kuehn GA, Schulson EM, Jones DE, Zhang J (1992) The compressive strength of ice cubes of different sizes. *J Offshore Mech Arct Eng* 115(2):349–356.
28. van Mier JGM (1986) Multiaxial strain-softening of concrete, Part I: Fracture. *Mater Struct* 19:179–190.
29. Mogi K (1962) The influence of the dimensions of specimens on the fracture strength of rocks. *Bull Earthquake Res Inst* 40:175–185.
30. del Viso JR, Carmona JR, Ruiz G (2008) Shape and size effects on the compressive strength of high-strength concrete. *Cement Concr Res* 38:386–395.
31. Pratt HR, Black AD, Brown WS, Brace WF (1972) The effect of specimen size on the mechanical properties of unjointed diorite. *Int J Rock Mech Min Sci* 9:513–529.
32. Bieniawski ZT (1968) The effect of specimen size on compressive strength of coal. *Int J Rock Mech Min Sci* 5(4):325–335.
33. Brace WF (1981) The effect of size on mechanical properties of rock. *Geophys Res Lett* 8(7):651–652.
34. Hoek E, Brown ET (1997) Practical estimates of rock mass strength. *Int J Rock Mech Min Sci* 34(8):1165–1186.
35. Bazant ZP, Xiang Y (1994) Compression failure of quasibrittle materials and size effect. *AMD-Vol. 185, Damage Mechanics in Composites* (ASME Winter Annual Meeting, Chicago, November, 1994), eds Allen DH, Ju JW, pp 143–148.
36. Herrmann HJ, Roux S (1990) *Statistical Models for the Fracture of Disordered Media* (North-Holland, Amsterdam).
37. Pradhan S, Hansen A, Chakrabarti BK (2010) Failure processes in elastic fiber bundles. *Rev Mod Phys* 82(1):499–555.
38. Delaplace A, Roux S, Pijaudier-Cabot G (1999) 'Damage cascade' in a softening interface. *Int J Solids Struct* 36(10):1403–1426.
39. Toussaint R, Pride SR (2002) Fracture of disordered solids in compression as a critical phenomenon. I. Statistical mechanics formalism. *Phys Rev E Stat Nonlin Soft Matter Phys* 66(3 Pt 2A):036135.
40. Toussaint R, Pride SR (2002) Fracture of disordered solids in compression as a critical phenomenon. II. Model Hamiltonian for a population of interacting cracks. *Phys Rev E Stat Nonlin Soft Matter Phys* 66(3 Pt 2A):036136.
41. Girard L, Amitrano D, Weiss J (2010) Fracture as a critical phenomenon in a progressive damage model. *J Stat Mech* 2010:P01013.
42. Girard L, Weiss J, Amitrano D (2012) Damage-cluster distributions and size effect on strength in compressive failure. *Phys Rev Lett* 108(22):225502.
43. Talamali M, Petäjä V, Vandembroucq D, Roux S (2012) Strain localization and anisotropic correlations in a mesoscopic model of amorphous plasticity. *C R Mec* 340(4–5):275–288.
44. Weiss J, Schulson EM (2009) Coulombic faulting from the grain scale to the geophysical scale: Lessons from ice. *J Phys D Appl Phys* 42:214017.
45. Eshelby JD (1957) The determination of the elastic field of an ellipsoidal inclusion, and related problems. *Proc R Soc A* 241:376–396.
46. Eshelby JD (1959) The Elastic field outside an ellipsoidal inclusion. *Proc R Soc A* 252:561–569.
47. Joanny JF, Degennes PG (1984) A model for contact-angle hysteresis. *J Chem Phys* 81(1):552–562.
48. Moulinet S, Rosso A, Krauth W, Rolley E (2004) Width distribution of contact lines on a disordered substrate. *Phys Rev E Stat Nonlin Soft Matter Phys* 69(3 Pt 2):035103.
49. Bonn D, Eggers J, Indekeu J, Meunier J, Rolley E (2009) Wetting and spreading. *Rev Mod Phys* 81(2):739–805.
50. Lemerle S, et al. (1998) Domain wall creep in an Ising ultrathin magnetic film. *Phys Rev Lett* 80(4):849–852.
51. Gao HJ, Rice JR (1989) A first-order perturbation analysis of crack trapping by arrays of obstacles. *J ApplMechTrans ASME* 56(4):828–836.
52. Santucci S, et al. (2007) Statistics of fracture surfaces. *Phys Rev E Stat Nonlin Soft Matter Phys* 75(1 Pt 2):016104.
53. Dalmas D, Lelarge A, Vandembroucq D (2008) Crack propagation through phase-separated glasses: Effect of the characteristic size of disorder. *Phys Rev Lett* 101(25):255501.
54. Bonamy D, Bouchaud E (2011) Failure of heterogeneous materials: A dynamic phase transition? *Phys Rep Rev Sec Phys Lett* 498(1):1–44.
55. Narayan O, Fisher DS (1993) Threshold critical dynamics of driven interfaces in random media. *Phys Rev B Condens Matter* 48(10):7030–7042.
56. Ertas D, Kardar M (1994) Critical dynamics of contact line depinning. *Phys Rev E Stat Phys Plasmas Fluids Relat Interdiscip Topics* 49(4):R2532–R2535.
57. Thuro K, Plinninger RJ, Zäh S, Schütz S (2001) Scale effects in rock strength properties. Part I: Unconfined compressive test and Brazilian test. *EUROCK 2001: Rock Mechanics - A Challenge for Society*, ed Sa E (Swets & Zeitlinger, Lisse, The Netherlands), pp 169–174.
58. Renshaw CE, Schulson EM (2001) Universal behaviour in compressive failure of brittle materials. *Nature* 412(6850):897–900.
59. Renshaw CE, Schulson EM (2004) Plastic faulting: Brittle-like failure under high confinement. *J Geophys Res* 109:B09207.
60. Habib P, Vouille G (1966) Sur la disparition de l'effet d'échelle aux hautes pressions [On the disparition of size effect under high confinement]. *C R Hebd Séanc Acad Sci Paris* 262:715–717. French.
61. Desrues J, Viggiani G (2004) Strain localization in sand: An overview of the experimental results obtained in Grenoble using stereophotogrammetry. *Int J Numer Anal Methods Geomech* 28(4):279–321.
62. Gimbert F, Amitrano D, Weiss J (2013) Crossover from quasi-static to dense flow regime in compressed frictional granular media. *EPL* 104:46001.
63. Radjai F, Dubois F (2011) *Discrete-Element Modelling of Granular Materials* (Wiley, Hoboken, NJ).
64. Agnolin I, Roux JN (2007) Internal states of model isotropic granular packings. I. Assembling process, geometry, and contact networks. *Phys Rev E Stat Nonlin Soft Matter Phys* 76(6 Pt 1):061302.
65. Talamali M, Petäjä V, Vandembroucq D, Roux S (2011) Avalanches, precursors, and finite-size fluctuations in a mesoscopic model of amorphous plasticity. *Phys Rev E Stat Nonlin Soft Matter Phys* 84(1 Pt 2):016115.

Supporting Information

Weiss et al. 10.1073/pnas.1403500111

SI Text

Here we (*i*) provide a formal derivation of the mapping of brittle compressive failure onto the depinning transition of an elastic manifold and (*ii*) present the characteristics and the simulation settings of the discrete-element model of frictional granular media.

Brittle Compressive Failure as a Depinning Transition

We consider a scalar field representing at a mesoscopic scale the damage in a geomaterial or the plastic strain in an amorphous material or a granular material. In quasi-static loading conditions, a simple and natural way of accounting for the nonlinear nature of the mechanisms that locally induce an irreversible change of structure consists of modeling its onset by threshold dynamics on the local stress state. Damage or plasticity occurs whenever the stress state $\boldsymbol{\sigma}$ reaches the boundary of an elastic domain defined by $F(\boldsymbol{\sigma}) = \sigma_c$. The heterogeneous nature of the material is accounted for by a statistical variability of the threshold σ_c.

The associated interplay between local disorder and elasticity is the basis of depinning models that have proved successful in recent years to describe various physical and mechanical phenomena. In all cases the modeling consists of reducing the problem to the motion of an elastic line (or manifold) in a random landscape. Let us denote $h(r, t)$ the location of the elastic line at time t. A general formulation of the equation of evolution in the framework of a depinning model thus reads (1)

$$\mathsf{M}\frac{\partial h}{\partial t}(\mathbf{r},t) = F_{\text{ext}}(t) + \int d\mathbf{r}' J(\mathbf{r} - \mathbf{r}')[h(\mathbf{r}',t) - h(\mathbf{r},t)] + \eta[\mathbf{r}, h(\mathbf{r},t)],$$

[S1]

where F_{ext} corresponds to an external driving force applied to the elastic line, M is a mobility coefficient, and η is a random noise characterized by its distribution and its spatial correlation accounting for the random nature of the material. The integral term is an elastic-like kernel depending on the phenomenon under study. The competition between elasticity and disorder in that framework is shown to induce a dynamic phase transition. Below some critical threshold, the elastic manifold advances only a finite distance before arresting. Above the threshold it can advance indefinitely and acquires a finite velocity. Close to the threshold typical critical features are recovered: divergence of a correlation length, finite size effects, etc. The application of this formalism has recently proved extremely useful in the field of solid mechanics. Models of interfacial crack propagation in mode I based on the early works of Gao and Rice (2) have enabled, for instance, the prediction of statistics of crack arrest lengths in indentation experiments (3) or the quantitative estimate of effective toughness of heterogeneous interfaces (4).

Here we propose to extend the depinning formalism to the case of compressive damage. As a starting point we discuss a model recently developed to describe plasticity of amorphous materials at a mesoscopic scale (5). In amorphous or disordered materials the development of plasticity or damage can be described as a series of local inelastic events (structural rearrangements or microcracks, respectively). In the first case, a local plastic strain ε_p can be associated to the mesoscale region where the rearrangement(s) has taken place; in the second case, a local damage D can represent the elastic weakening induced by the microcracks at the mesoscale. In both cases the occurrence of an event can be associated to the satisfaction of a criterion based on the value of the local stress field $F(\boldsymbol{\sigma}) = \sigma_c$, where the random nature of σ_c accounts for the material disorder. In both cases, the occurrence of a local

inelastic event in an elastic matrix (the remainder of the material) is responsible for an internal stress field. The modeling of this internal stress field is a key ingredient in the development of the model.

The internal stress field induced by an inelastic event can obviously be computed numerically as detailed below in *Discrete-Element Model of Frictional Granular Media*. It will depend on the fine details of the inelastic event as well as the elastic matrix. However, far from the rearrangement only the asymptotic far field will really matter. In the present framework of building a depinning model at mesoscopic scale, we concentrate on the asymptotic far field and forget about the finer details.

In two of the most influential papers ever published in solid mechanics, Eshelby calculated the stress field induced by an ellipsoidal inclusion (6, 7). It appears that in the far field the elastic interaction scales as r^{-d}, where r is the distance and d the topological dimension. This interaction exhibits an anisotropic character: In some directions the stress is enhanced whereas in others it is decreased. This anisotropy of the elastic interaction is a key ingredient of the modeling of the localization behavior in amorphous plasticity as in damage. More specifically, Eshelby solved two different inclusion problems. The first one, also known as the eigenstrain problem, consists of finding the elastic stress induced by a deformed inclusion in an elastic matrix. In this case both inclusion and matrix are made of the same material. This case naturally applies to an inclusion that has undergone plastic deformation. It also applies, with some simplifying assumptions, to the case of granular media undergoing irreversible local rearrangements of the granular structure (*Discrete-Element Model of Frictional Granular Media*). The second problem, known as the inhomogeneity problem, consists of finding the elastic stress induced in an elastic matrix under remote loading by an inclusion characterized by elastic properties different from those of the matrix. This case applies to an inclusion that has undergone local damage.

Plastic Inclusions and Amorphous Plasticity. For the sake of simplicity we restrict to the case of a 2D problem (e.g., plane strain). In the absence of inclusion we consider a biaxial loading characterized by σ_x^{ext} and σ_y^{ext}. The material is characterized by a Young modulus E and a Poisson coefficient v. Let us now consider a unique circular inclusion of radius λ. The inclusion is located at the origin and polar coordinates are used.

We first specialize to the case of plasticity (the first Eshelby problem). The inclusion has undergone plastic deformation that in absence of the matrix would result in a local plastic (purely deviatoric) strain ε_p. Assuming that the symmetry of this local plastic strain is the same as the external loading, we obtain for the elastic perturbation (e.g., ref. 8)

$$\sigma_{xx} - \sigma_{yy} = \Lambda \frac{E}{1-v^2} \frac{\lambda^2 \langle \varepsilon_p \rangle \cos(4\theta)}{r^2}$$

$$\sigma_{xy} = \Lambda \frac{E}{1-v^2} \frac{\lambda^2 \langle \varepsilon_p \rangle \sin(4\theta)}{r^2} \qquad \textbf{[S2]}$$

$$\sigma_{xx} + \sigma_{yy} = \Lambda \frac{E}{1-v^2} \frac{\lambda^2 \langle \varepsilon_p \rangle \cos(2\theta)}{r^2},$$

where Λ is a constant depending on v. A crucial point here is that whatever the precise shape of the reorganized region is, the far-field asymptotics will remain unchanged, with an amplitude proportional to the surface $S = \pi\lambda^2$ of an equivalent spherical inclusion times the mean plastic deformation ε_p it would have undergone in the absence of a surrounding matrix.

Note here another crucial point: In this first case of amorphous plasticity, matrix and inclusion are characterized by the same elastic properties. The case of multiple inclusions is thus immediately solved by superposition.

In this framework, assuming a scalar plastic criterion based on the sole local shear stress $\tau = |\sigma_{xx} - \sigma_{yy}|$, a simple equation of evolution for the plastic strain ε_p can be written in the framework of a quasi-static loading, considering an overdamped dynamics (5)

$$\mathsf{M}\frac{\partial \varepsilon_p(\mathbf{r},t)}{\partial t} = \mathcal{R}\left[\tau^{\text{ext}}(t) + \tau^{\text{el}}(\mathbf{r},\{\varepsilon_p\}) - \tau_c(\mathbf{r},\varepsilon_p)\right], \quad \textbf{[S3]}$$

where $\mathcal{R}$ denotes the positive part, and

$$\tau^{\text{el}}(\mathbf{r},\{\varepsilon_p\}) = A \int \frac{\cos(4\theta_{rr'})}{|\mathbf{r}-\mathbf{r}'|^2}\left[\varepsilon_p(\mathbf{r}',t) - \varepsilon_p(\mathbf{r},t)\right]d\mathbf{r}'. \quad \textbf{[S4]}$$

One recovers here a typical depinning model, consistent with the general definition given above in [S1] with an external driving "force" τ^{ext}, a random field τ_c, and an elastic kernel τ^{el}. Note here that in contrast to most depinning models, the elastic kernel is anisotropic, which induces a specific localization behavior to the model (5). To complete the depinning interpretation we can embed the 2D lattice in a 3D space where the extra coordinate is given by the plastic strain ε_p. In so doing we recover the motion of a 2D manifold in a 3D random landscape.

Compressive Damage: From Elastic Inhomogeneities to Stress Fluctuations.
We discuss now the case of a circular inhomogeneity of radius λ, of Young modulus $E_1 = E_0(1-D)$, where D is the local damage, and (for the sake of simplicity) of unchanged Poisson coefficient v. In plane strain we note $\kappa = 3-4v$. We consider a remote biaxial stress characterized by σ_x^{ext} and σ_y^{ext}. The far-field internal stress induced by the inhomogeneity reads

$$\sigma_{xx} + \sigma_{yy} = \frac{-2D}{1+\kappa(1-D)}\frac{\lambda^2\left(\sigma_x^{\text{ext}} - \sigma_y^{\text{ext}}\right)\cos(2\theta)}{r^2}$$

$$\sigma_{xx} - \sigma_{yy} = \frac{-2D}{1+\kappa(1-D)}\frac{\lambda^2\left(\sigma_x^{\text{ext}} - \sigma_y^{\text{ext}}\right)\cos(4\theta)}{r^2}$$

$$+ \frac{1}{2}\frac{D}{1+2(1-D)/(\kappa-1)}\frac{\lambda^2\left(\sigma_x^{\text{ext}} + \sigma_y^{\text{ext}}\right)\cos(2\theta)}{r^2} \quad \textbf{[S5]}$$

$$\sigma_{xy} = \frac{-D}{1+\kappa(1-D)}\frac{\lambda^2\left(\sigma_x^{\text{ext}} - \sigma_y^{\text{ext}}\right)\sin(4\theta)}{r^2}$$

$$+ \frac{1}{4}\frac{D}{1+2(1-D)/(\kappa-1)}\frac{\lambda^2\left(\sigma_x^{\text{ext}} + \sigma_y^{\text{ext}}\right)\sin(2\theta)}{r^2}.$$

This gives in a more condensed form

$$\sigma_{xx} + \sigma_{yy} = \left(\sigma_x^{\text{ext}} - \sigma_y^{\text{ext}}\right)f(D)B_2\left(\frac{r}{\lambda},\theta\right)$$

$$\sigma_{xx} - \sigma_{yy} = \left(\sigma_x^{\text{ext}} - \sigma_y^{\text{ext}}\right)f(D)B_4\left(\frac{r}{\lambda},\theta\right) + \left(\sigma_x^{\text{ext}} + \sigma_y^{\text{ext}}\right)g(D)B_2\left(\frac{r}{\lambda},\theta\right)$$

$$\sigma_{xy} = \frac{1}{2}\left(\sigma_x^{\text{ext}} - \sigma_y^{\text{ext}}\right)f(D)C_4\left(\frac{r}{\lambda},\theta\right)$$

$$+ \frac{1}{2}\left(\sigma_x^{\text{ext}} + \sigma_y^{\text{ext}}\right)g(D)C_2\left(\frac{r}{\lambda},\theta\right), \quad \textbf{[S6]}$$

where the functions B and C present an inverse quadratic dependence with distance and the indexes 2 and 4 denote the di-

polar and quadrupolar symmetries, respectively. Note that for small values of D, functions f and g can be regarded as almost linear.

How do we extend this result, obtained with an isolated inhomogeneity, to the stress induced by a damage field $D(\mathbf{r})$? The disordered material can be here regarded as a set of inhomogeneities of size λ, the discretization scale of the model. In contrast to the case of plasticity, the generalization to a large number of inhomogeneities is not immediate because of interactions between them and so simple superposition is not exact here. Our approximation consists of considering that the internal stress field results from a superposition of the stresses induced by individual inclusions embedded in an equivalent matrix of effective modulus (at the macroscale) $\overline{E} = E_0(1-\overline{D})$, where E_0 is the initial Young modulus of the material and $\overline{D}$ is the effective mean damage.

Before detailing our approach, it is of interest to briefly discuss the question of the elastic behavior of disordered materials and its implication for damage. Historically, mechanical engineering studies have focused on homogenization, i.e., the determination of the average elastic properties at a macroscopic scale from the knowledge of the microscopic properties. Conversely, statistical physics studies mainly focused on the stress fluctuations induced by the elastic disorder. Here we consider the evolution with damage of both the mean elastic behavior and its fluctuations.

Consider the material at a given stage of damage. The damage field $D(\mathbf{r})$ gives immediate access to the heterogeneous elastic properties, $E(\mathbf{r}) = E_0[1 - D(\mathbf{r})]$. Here and in the following (for the sake of simplicity) the Poisson coefficient ν is assumed to remain unchanged. From this knowledge, an effective (average) Young modulus $\overline{E}$ can be defined at a macroscopic scale. A fluctuating damage field $D^{\text{fluc}}(\mathbf{r})$ can thus be defined from the contrast between the actual elastic moduli at a microscopic scale $E(\mathbf{r})$ and the effective (average) modulus $\overline{E}$ at a macroscopic scale. Stress fluctuations can be then obtained from this fluctuating damage field.

What is the effect of the occurrence of a localized damage event in this framework? At first it will affect (weaken) the average elastic behavior: Effective moduli will undergo a slight decrease. As a direct consequence of this evolution of the average elastic behavior, stress fluctuations induced by the stiffer (less damaged than average) regions will be amplified because the contrast with the effective matrix has increased. Conversely, stress fluctuations induced by the softer (more damaged than average) regions will be attenuated. On top of that, the newly damaged area will give an additional contribution to the stress fluctuations.

This sets the theoretical framework of our approach. No particular approximation has been performed so far because the methods to be used for the determination of the effective modulus $\overline{E}$ and the stress fluctuations remain to be specified. Note in particular that interactions between inhomogeneities can affect the determination of both the effective moduli and the stress fluctuations. To be more specific and make possible a future numerical implementation (out of the scope of the present study), a natural choice would consist of resorting to a self-consistent approximation for the computation of the effective modulus $\overline{E}$ and to a simple superposition of isolated inhomogeneities within the just-defined effective matrix to compute the stress fluctuations. In so doing the internal stress is thus obtained through two successive steps: (*i*) the determination of the Young modulus $\overline{E}$ of the effective matrix associated to a given damage field $D(\mathbf{r})$ and (*ii*) the computation of the stress fluctuations from isolated "effective" inhomogeneities due to the contrast between the local moduli $E(r)$ and the effective modulus $\overline{E}$. Here the self-consistent scheme proposed for step *i* partly accounts for interactions between inhomogeneities whereas for step *ii* these interactions are not explicitly accounted for, but only via the value of the effective modulus $\overline{E}$ that sets the precise level of elastic contrast of each inhomogeneity.

Using the effective mean damage $\overline{D}$ that derives from the self-consistent estimate of the effective modulus $\overline{E} = E_0(1-\overline{D})$, we

define the fluctuating damage field $D^{\text{fluc}}(\mathbf{r})$ that gives the local contrast to the effective matrix:

$$D^{\text{fluc}}(\mathbf{r}) = \frac{D(\mathbf{r}) - \overline{D}}{1 - \overline{D}}. \qquad \textbf{[S7]}$$

We can now write the internal stress induced by the damage field $D(\mathbf{r})$ as a superposition of the stress fields radiated by the local inhomogeneities $D^{\text{fluc}}(\mathbf{r})$ within the homogeneous matrix of modulus $\overline{E}$:

$$\sigma_{xx}^{\text{el}}(\mathbf{r}) + \sigma_{yy}^{\text{el}}(\mathbf{r}) = \left(\sigma_x^{\text{ext}} - \sigma_y^{\text{ext}}\right) \int f\left[D^{\text{fluc}}(\mathbf{r}') - D^{\text{fluc}}(\mathbf{r})\right] B_2\left(\frac{|\mathbf{r} - \mathbf{r}'|}{\lambda}, \theta_{r,r'}\right) d\mathbf{r}'$$

$$\sigma_{xx}^{\text{el}}(\mathbf{r}) - \sigma_{yy}^{\text{el}}(\mathbf{r}) = \left(\sigma_x^{\text{ext}} - \sigma_y^{\text{ext}}\right) \int f\left[D^{\text{fluc}}(\mathbf{r}') - D^{\text{fluc}}(\mathbf{r})\right] B_4\left(\frac{|\mathbf{r} - \mathbf{r}'|}{\lambda}, \theta_{r,r'}\right) d\mathbf{r}'$$
$$+ \left(\sigma_x^{\text{ext}} + \sigma_y^{\text{ext}}\right) \int g\left[D^{\text{fluc}}(\mathbf{r}') - D^{\text{fluc}}(\mathbf{r})\right] B_2\left(\frac{|\mathbf{r} - \mathbf{r}'|}{\lambda}, \theta_{r,r'}\right) d\mathbf{r}'$$
$$\textbf{[S8]}$$

$$\sigma_{xy}^{\text{el}}(\mathbf{r}) = \frac{1}{2}\left(\sigma_x^{\text{ext}} - \sigma_y^{\text{ext}}\right) \int f\left[D^{\text{fluc}}(\mathbf{r}') - D^{\text{fluc}}(\mathbf{r})\right] C_4\left(\frac{|\mathbf{r} - \mathbf{r}'|}{\lambda}, \theta_{r,r'}\right) d\mathbf{r}'$$
$$+ \frac{1}{2}\left(\sigma_x^{\text{ext}} + \sigma_y^{\text{ext}}\right) \int g\left[D^{\text{fluc}}(\mathbf{r}') - D^{\text{fluc}}(\mathbf{r})\right] C_2\left(\frac{|\mathbf{r} - \mathbf{r}'|}{\lambda}, \theta_{r,r'}\right) d\mathbf{r}'.$$

Compressive Damage: Stress-Based Criterion. We use the Coulomb criterion, $|\tau| + \mu\sigma_N = \tau_C$, to define the onset of damage, with $\mu = \tan(\varphi)$ the internal friction coefficient and φ the angle of internal friction. This criterion can be rewritten as a function of the eigenvalues of the stress tensor $\sigma_1 > \sigma_2$ as (9)

$$F(\sigma) = (\sigma_1 - \sigma_2) + (\sigma_1 + \sigma_2)\sin(\varphi) - 2\cos(\varphi)\tau_C = 0. \qquad \textbf{[S9]}$$

To map this compressive damage problem onto a depinning model, we rewrite this last expression for a biaxial stress state perturbed by the elastic contributions induced by the damage field, $\sigma = \sigma^{\text{ext}} + \sigma^{\text{el}}$. This requires the computation of the eigenvalues σ_1 and σ_2, which are obtained from

$$\sigma_1 + \sigma_2 = \left(\sigma_x^{\text{ext}} + \sigma_y^{\text{ext}}\right) + \left(\sigma_{xx}^{\text{el}} + \sigma_{yy}^{\text{el}}\right) \qquad \textbf{[S10]}$$

and

$$(\sigma_1 - \sigma_2)^2 = \left(\sigma_x^{\text{ext}} - \sigma_y^{\text{ext}}\right)^2 + 2\left(\sigma_x^{\text{ext}} - \sigma_y^{\text{ext}}\right)\left(\sigma_{xx}^{\text{el}} - \sigma_{yy}^{\text{el}}\right) + \left(\sigma_1^{\text{el}} - \sigma_2^{\text{el}}\right)^2. \qquad \textbf{[S11]}$$

Note that we expect σ^{el} to be of the order of $\epsilon \times \sigma^{\text{ext}}$, where the magnitude small parameter ϵ should be given by the typical value of damage (relative fluctuation of the elastic modulus). Restricting our calculation to first order and replacing the internal stress by a superposition of Eshelby stresses induced by effective inhomogeneities as derived above, we obtain

$$\sigma_1 + \sigma_2 = \left(\sigma_x^{\text{ext}} + \sigma_y^{\text{ext}}\right) + \left(\sigma_x^{\text{ext}} - \sigma_y^{\text{ext}}\right)\mathcal{A}_2 \qquad \textbf{[S12]}$$

and

$$(\sigma_1 - \sigma_2)^2 = \left(\sigma_x^{\text{ext}} - \sigma_y^{\text{ext}}\right)^2 + 2\left(\sigma_x^{\text{ext}} - \sigma_y^{\text{ext}}\right)^2 \mathcal{B}_4$$
$$+ 2\left(\sigma_x^{\text{ext}} - \sigma_y^{\text{ext}}\right)\left(\sigma_x^{\text{ext}} + \sigma_y^{\text{ext}}\right)\mathcal{B}_2 + O(\epsilon^2), \qquad \textbf{[S13]}$$

which gives

$$\sigma_1 - \sigma_2 = \left(\sigma_x^{\text{ext}} - \sigma_y^{\text{ext}}\right)(1 + \mathcal{B}_4) + \left(\sigma_x^{\text{ext}} + \sigma_y^{\text{ext}}\right)\mathcal{B}_2 + O(\epsilon^2), \qquad \textbf{[S14]}$$

where

$$\mathcal{A}_2\left[\{D\}, \frac{\mathbf{r}}{\lambda}\right] = \int f\left[D^{\text{fluc}}(\mathbf{r}') - D^{\text{fluc}}(\mathbf{r})\right] B_2\left(\frac{|\mathbf{r} - \mathbf{r}'|}{\lambda}, \theta_{r,r'}\right) d\mathbf{r}'$$

$$\mathcal{B}_2\left[\{D\}, \frac{\mathbf{r}}{\lambda}\right] = \int g\left[D^{\text{fluc}}(\mathbf{r}') - D^{\text{fluc}}(\mathbf{r})\right] B_2\left(\frac{|\mathbf{r} - \mathbf{r}'|}{\lambda}, \theta_{r,r'}\right) d\mathbf{r}'$$

$$\mathcal{B}_4\left[\{D\}, \frac{\mathbf{r}}{\lambda}\right] = \int f\left[D^{\text{fluc}}(\mathbf{r}') - D^{\text{fluc}}(\mathbf{r})\right] B_4\left(\frac{|\mathbf{r} - \mathbf{r}'|}{\lambda}, \theta_{r,r'}\right) d\mathbf{r}'.$$

We can now rewrite the Coulomb criterion

$$F(\sigma) = \left(\sigma_x^{\text{ext}} - \sigma_y^{\text{ext}}\right) + \left(\sigma_x^{\text{ext}} + \sigma_y^{\text{ext}}\right)\sin(\varphi) + \left(\sigma_x^{\text{ext}} - \sigma_y^{\text{ext}}\right)\mathcal{B}_4$$
$$+ \left(\sigma_x^{\text{ext}} + \sigma_y^{\text{ext}}\right)\mathcal{B}_2 + \left(\sigma_x^{\text{ext}} - \sigma_y^{\text{ext}}\right)\mathcal{A}_2\sin(\varphi) - 2\cos(\varphi)\tau_C \qquad \textbf{[S15]}$$

or in a more condensed way

$$F(\sigma) = \sigma_s^{\text{ext}} + \sigma_s^{\text{el}}\left(\{D\}, \frac{\mathbf{r}}{\lambda}\right) - 2\cos(\varphi)\tau_C(\mathbf{r}), \qquad \textbf{[S16]}$$

where $\tau_C(\mathbf{r})$ is the spatially fluctuating cohesion [note that we may have also the cohesion depending on the damage field, $\tau_C(\{D\}, \mathbf{r})$, if the disorder is not fully quenched], and

$$\sigma_s^{\text{ext}} = \left(\sigma_x^{\text{ext}} - \sigma_y^{\text{ext}}\right) + \left(\sigma_x^{\text{ext}} + \sigma_y^{\text{ext}}\right)\sin(\varphi)$$

$$\sigma_s^{\text{el}}\left(\{D\}, \frac{\mathbf{r}}{\lambda}\right) = \left(\sigma_x^{\text{ext}} - \sigma_y^{\text{ext}}\right)\mathcal{B}_4\left(\{D\}, \frac{\mathbf{r}}{\lambda}\right) + \left(\sigma_x^{\text{ext}} + \sigma_y^{\text{ext}}\right)\mathcal{B}_2\left(\{D\}, \frac{\mathbf{r}}{\lambda}\right)$$
$$+ \left(\sigma_x^{\text{ext}} - \sigma_y^{\text{ext}}\right)\mathcal{A}_2\left(\{D\}, \frac{\mathbf{r}}{\lambda}\right)\sin(\varphi).$$

Combining these expressions with [S16], we can now write a simple equation of evolution of the damage field based on the positive part of the yield function $F(\sigma)$. The damaging rate is assumed to linearly depend on the excess of the local stress with respect to the Coulomb stress. As detailed above, the local stress is a sum of two contributions, the externally imposed stress and an internal stress that depends on the full damage field. We thus recover a complete mapping onto a depinning model, with the following equation of evolution of the damage field,

$$\mathsf{M}\frac{\partial D}{\partial t}(\mathbf{r}) = \mathcal{R}\left[\sigma_s^{\text{ext}} + \sigma_s^{\text{el}}\left(\{D\}, \overline{E}(\{D\}), \frac{\mathbf{r}}{\lambda}\right) - 2\cos(\varphi)\tau_C(\mathbf{r}, D)\right], \qquad \textbf{[S17]}$$

where $\mathcal{R}$ denotes, as above, the positive part. We identify σ_s^{ext} as the external forcing term, σ_s^{el} as the elastic contribution induced by the damage field D, and τ_C the disorder. In [S17], we have made explicit the dependence of the internal stress σ_s^{el} on the modulus $\overline{E}$ of the effective elastic matrix to make more apparent the two successive steps of its computation (self-consistent estimate of the modulus of the effective matrix and superposition of the elastic interactions induced by isolated inhomogeneities within the effective matrix).

Following Eq. **S16** a stress threshold $\sigma_C = 2\tau_C \cos(\varphi)$ can be defined. The fluctuations of the local stress threshold $\delta\sigma_C = 2\delta\tau_C \cos(\varphi)$ give a natural scale for the stress fluctuations within the material. We thus expect the characteristic lengths L_A and L_B to be dressed with a parameter that depends on $\delta\sigma_C$. λ being the characteristic length scale of the disorder (i.e., the discretization scale of our mesoscopic model), we thus expect the strength fluctuations to scale as $\delta(\sigma_f)/\sigma_\infty = C(\delta\tau_c/\tau_c)(L/\lambda)^{-1/\nu_{\mathrm{FS}}}$ and the length scales L_A and L_B as $L_{A,B} \sim \lambda(\delta\tau_c/\tau_c)^{\nu_{\mathrm{FS}}}$. In the case of strong disorder $\delta\tau_c \gg \tau_c$ these length scales can thus be significantly larger than λ.

This description of the internal stress field induced by the progressive damage as a simple superposition of the stress fields induced by isolated inhomogeneities within an effective matrix is obviously only approximate. Two limitations may be emphasized at this stage. First, the asymptotic field cannot be reduced to the effect of an equivalent spherical inclusion and also depends on the shape (10, 11). In the presence of cracks, we expect, for instance, anisotropic effects that are not accounted for in the present modeling. In particular, the homogeneous effective matrix (used here as an intermediate step to compute the internal stress) can be anisotropic whereas it has been considered here as isotropic. Moreover, as damage is progressive, the matrix to be considered around the inclusion is itself already damaged. As proposed above, one may use an effective modulus to account for the weakening. Still an important feature will be missed: the asymmetry of the elastic properties of the damaged matrix between loading and unloading. This question has been discussed by Roux and Hild (12), who analyzed the behavior of the elastic influence function along the damage process. They show that this influence function can still be described as a power law of the distance to the crack or inclusion but with an exponent that depends on the state of damage and that eventually approaches mean-field interaction.

As already mentioned in the main text, the case of a cohesionless frictional granular medium compressed under confinement can be interpreted as an intermediate case between the amorphous plasticity and compressive damage problems. This frictional granular material may be described by Eq. **S17** derived above for the evolution of damage, replacing the damage variable D by the plastic strain variable ε_p and using for the elastic stress the same strategy as above, starting from Eq. **S2** (homogeneous Eshelby) instead of Eq. **S5** (inhomogeneous Eshelby). Numerical simulations are necessary for a complete description, as detailed in *Discrete-Element Model of Frictional Granular Media* below.

Within the approximations discussed above, amorphous plasticity as well as compressive damage can be discussed in the theoretical framework of a depinning model (Eqs. **S3** and **S17**). By construction such models exhibit a dynamical phase transition. Below a critical value of the applied external stress, the material experiences only limited damage (or plastic deformation) and its structural integrity remains. The closer the external stress is to threshold, the larger the extent of damage. Failure (or plastic flow) is eventually obtained once the critical threshold is reached. This description of mechanical failure as a critical phase transition implies the presence of traditional features of criticality, in particular the divergence of a correlation length and universal statistics of finite size effects (13–15), as detailed in the main text. In addition, the anisotropic character of the elastic kernels associated with Eshelby inclusions naturally induces a localization behavior (5).

Discrete-Element Model of Frictional Granular Media

Simulations of the mechanical behavior of granular materials were performed using the molecular dynamics discrete element method (16). The main characteristics of the model, which has been described in more detail elsewhere (17), are summarized below.

Two-dimensional granular assemblies made of a set of N_g frictional circular grains were considered. The dynamic equa-

tions are solved for each of the grains, which interact via linear elastic laws and Coulomb friction when they are in contact (18). The normal contact force f_n is related to the normal apparent interpenetration δ_n of the contacts as $f_n = k_n \times \delta_n$, where k_n is the normal contact stiffness coefficient ($\delta_n > 0$ if a contact is present, and $\delta_n = 0$ if there is no contact). The tangential component f_t of the contact force is proportional to the tangential elastic relative displacement, with a tangential stiffness coefficient k_t. Here we set $k_t = k_n$. Neither cohesion between grains nor rolling resistance is considered. The Coulomb condition $|f_t| \leq \mu_{\mathrm{micro}}$, where μ_{micro} is the grain friction coefficient, requires an incremental evaluation of f_t every time step, which leads to some amount of slip each time one of the equalities $f_t = \pm\mu_{\mathrm{micro}} \times f_n$ is reached. A normal viscous component opposing the relative normal motion of any pair of grains in contact is also added to the elastic force f_n to obtain a damping of the dynamics.

All of the granular assemblies built for the present work were obtained under static loading in the absence of body forces (such as gravity). Circular 2D grains of uniformly distributed surfaces are considered. The polydispersity is kept constant for all samples, setting the largest grain diameter $D_{\max}$ such that $D_{\max} = 3D_{\min}$.

Sample Preparation. The particles are randomly (in terms of diameter) placed on sites of a regular lattice of spacing $D_{\max}$, before being mixed. This mixing procedure uses the contact dynamics (CD) method (16), so considers hard disks, and consists in setting grains in motion with random velocities, leaving them to interact in collisions that preserve kinetic energy, to produce a disordered configuration. At the end of this procedure, all grains velocities are set equal to 0 and an isotropic compression is performed using the molecular dynamics (MD) method.

This isotropic compression step of sample preparation is here performed in two different ways, and three different types of initial samples named highly coordinated (HC), low-coordinated 1 (LC1), and LC2 differing in packing fraction and coordination number are built as explained in the following. The results shown in Fig. 3 of the main text correspond to the intermediate configuration LC1.

HC samples. HC and very dense samples are obtained from an isotropic compression on frictionless grains, i.e., setting a particle friction value $\mu_{\mathrm{iso}} = 0$. The samples built in that case show values of initial packing density Φ_{ini} of the order of 0.847 ± 0.001 and a backbone coordination number, i.e., average number of contacts by grain that carry forces, $Z^*_{\mathrm{ini}} = 4$.

Initially LC samples. LC samples, characterized by Z^*_{ini} of the order of 3, are obtained following the method of ref. 18, i.e., by maintaining strongly agitated granular gas states at high densities before performing the isotropic compression with a final value of friction coefficient. Contrary to ref. 18, shaking is here performed at various distances from the maximum packing fraction (obtained from *HC samples*), by tuning the expansion parameter α. Details of the procedure, starting from a disordered granular gas, are as follows:

First, an isotropic compression is performed on frictionless particles until reaching an equilibrium state of maximum packing fraction, as done in *HC samples*).

Second, a homogeneous expansion, multiplying all coordinates by a constant factor α slightly larger than 1, is performed. Two values for α, which both lead to an expansion greater than the maximum grain interpenetration, are taken into account in this study. We considered $\alpha = 1.01$ to build samples of type LC1, which are characterized by packing densities similar to the samples obtained in *HC samples*, i.e., Φ_{ini} of the order of 0.847 ± 0.001 and $\alpha = 1.1$ to build samples of type LC2, which are characterized by smaller packing densities of $\Phi_{\mathrm{ini}} = 0.82 \pm 0.002$.

Third, a shaking procedure that uses the same contact dynamics code as the one used during the preparation of the granular gas is performed. The number of iterations n_{it} is imposed to be constant for all samples generated. Here, we set $n_{it} = 5 \times 10^5$, which corresponds to the lower bound value above which the values of Φ_{ini} and Z^*_{ini} obtained at the end of the sample preparation are not affected by the values of n_{it}.

Finally, an isotropic compression setting the particle friction $\mu_{iso} = \mu_{biax} = 1$ is performed, where $\mu_{biax} = 1$ is the particle friction considered during the multiaxial testing explained in the following.

Multiaxial loading configuration. An increase of the external axial stress σ_1 is prescribed to impose the constant axial strain rate (see below), whereas the radial stress σ_3, i.e., the confining pressure, is kept constant. The external mechanical loading is prescribed on the grain assembly, using periodic boundary conditions. Instead of considering a sample delimited by rigid walls on which force is applied at the boundary of the sample, which would lead to an inhomogeneous repartition of the external force through the granular assembly (16), we consider a periodic simulation cell.

The grain stiffness coefficient $k_t = k_n$ and the confining pressure σ_3 are sized with respect to the contact stiffness $K = k_n/\sigma_3$ that we set equal to 1,000. This value for K is of the order of the one obtained in a compression experiment performed on glass bead assemblies under 100 kPa of confining pressure, where K approximately equals 3,000 in that case.

The axial strain ε is imposed to increase at a constant rate by prescribing a constant strain increment $\delta\varepsilon_1$ at each discretization time interval. To ensure quasi-static loading, $\delta\varepsilon_1$ is sized with

respect to the inertial number I defined as $I = \dot{\varepsilon}_1\sqrt{\overline{m}/\sigma_3}$, where $\overline{m}$ is the average grain mass. We here set $I = 5 \times 10^{-5}$, ensuring quasi-static loading (16, 19).

As for the multiaxial compression tests on coal discussed in Fig. 2, the deviatoric stress $\sigma_1 - \sigma_3$ has been considered here as the relevant variable.

Simulations. Simulations were performed for various sample sizes defined as $L = \sqrt{N_g}$. We made L to vary from 10 to 212. The number of independent simulations performed with each system size has been set equal to 100, except for the largest system size $L = 212$ for which only 20 simulations have been performed.

The sample preparation procedure described above is a way to set different levels of initial disorder, allowing us to check the robustness of our size-effect formalism against this disorder level. In other words, disorder is not introduced in an *ad hoc* manner, but rather has a topological origin that is physically materialized at the microscopic scale by changes in the spatial organization of grains and grain contacts. This initial topological disorder has a strong influence on macroscopic behavior: The HC samples appear much stiffer than LC samples, with a brutal postinstability softening. Despite these strongly different macroscopic responses, the size effects on yield stress are very well described by our formalism (Eqs. **1** and **2** of the main text) for HC, LC1, and LC2 samples, with an exponent ν_{FS} that is very close to 1 in all cases (Table S1), in agreement with the mean-field exponent ν of the depinning transition (20). On the contrary, the disorder plays a significant role on asymptotic strength, with a larger σ_∞ for highly coordinated, dense samples, as expected. The scales L_A and L_B are slightly larger than the average particle size and increase for less dense, less coordinated samples, as expected.

1. Fisher DS, Dahmen K, Ramanathan S, Ben-Zion Y (1997) Statistics of earthquakes in simple models of heterogeneous faults. *Phys Rev Lett* 78(25):4885–4888.
2. Gao HJ, Rice JR (1989) A first-order perturbation analysis of crack trapping by arrays of obstacles. *J Appl Mech Trans ASME* 56(4):828–836.
3. Charles Y, Hild F, Roux S, Vandembroucq D (2006) Material-independent crack arrest statistics: Application to indentation experiments. *Int J Fract* 142(1–2):51–67.
4. Patinet S, Vandembroucq D, Roux S (2013) Quantitative prediction of effective toughness at random heterogeneous interfaces. *Phys Rev Lett* 110(16):165507.
5. Talamali M, Petäjä V, Vandembroucq D, Roux S (2012) Strain localization and anisotropic correlations in a mesoscopic model of amorphous plasticity. *C R Mec* 340(4–5):275–288.
6. Eshelby JD (1957) The determination of the elastic field of an ellipsoidal inclusion, and related problems. *Proc R Soc A* 241:376–396.
7. Eshelby JD (1959) The elastic field outside an ellipsoidal inclusion. *Proc R Soc A* 252:561–569.
8. Gong SX, Meguid SA (1993) Interacting circular inhomogeneities in plane elastostatics. *Acta Mech* 99(1–4):49–60.
9. Jaeger JC, Cook NGW (1979) *Fundamentals of Rock Mechanics* (Chapman & Hall, London).
10. Sevostianov I, Kachanov M (2011) Elastic fields generated by inhomogeneities: Far-field asymptotics, its shape dependence and relation to the effective elastic properties. *Int J Solids Struct* 48(16–17):2340–2348.
11. Sevostianov I, Kachanov M (2012) Is the concept of "average shape" legitimate, for a mixture of inclusions of diverse shapes? *Int J Solids Struct* 49(23–24):3242–3254.
12. Roux S, Hild F (2002) On the relevance of mean field to continuum damage mechanics. *Int J Fract* 116(3):219–229.
13. Baret JC, Vandembroucq D, Roux S (2002) Extremal model for amorphous media plasticity. *Phys Rev Lett* 89(19):195506.
14. Girard L, Amitrano D, Weiss J (2010) Fracture as a critical phenomenon in a progressive damage model. *J Stat Mech* 2010:P01013.
15. Girard L, Weiss J, Amitrano D (2012) Damage-cluster distributions and size effect on strength in compressive failure. *Phys Rev Lett* 108(22):225502.
16. Radjai F, Dubois F (2011) *Discrete-Element Modelling of Granular Materials* (Wiley, Hoboken, NJ).
17. Gimbert F, Amitrano D, Weiss J (2013) Crossover from quasi-static to dense flow regime in compressed frictional granular media. ArXiv:1208.1930.v3.
18. Agnolin I, Roux JN (2007) Internal states of model isotropic granular packings. I. Assembling process, geometry, and contact networks. *Phys Rev E Stat Nonlin Soft Matter Phys* 76(6 Pt 1):061302.
19. GDR MiDi (2004) On dense granular flows. *Eur Phys J E Soft Matter* 14(4):341–365.
20. Ertas D, Kardar M (1994) Critical dynamics of contact line depinning. *Phys Rev E Stat Phys Plasmas Fluids Relat Interdiscip Topics* 49(4):R2532–R2535.
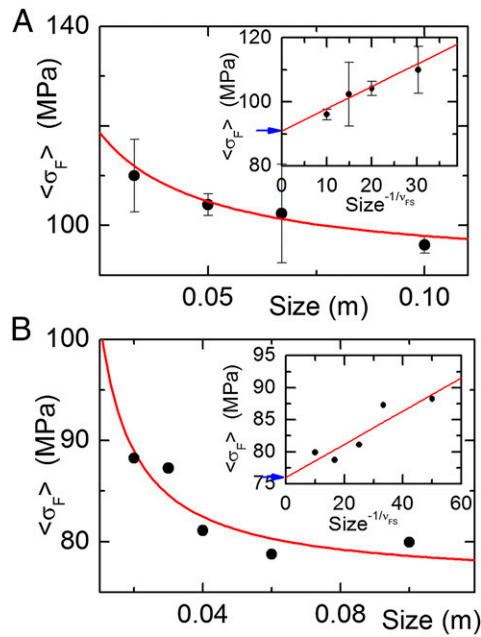
Fig. S1. (*A* and *B*) Finite-size effect on uniaxial compressive strength for HP concrete (1) (*A*) and marble (2) (*B*). Main graphs: mean compressive strength σ_f vs. size. Black circles: published experimental data, with associated SD (when reported). Red curve: fit by Eq. **3** of the main text, using $\nu_{FS} = 1$. The best-fit asymptotic strengths σ_∞ are 91 MPa for HP concrete and 76 MPa for marble. The associated scales L_B are, respectively, 7.6 mm and 3.4 mm. Insets show same data and fits, in a σ_f vs. $L^{-1/\nu_{FS}}$ graph, where Eq. **3** is a straight line and reveals the asymptotic strength σ_∞.

1. del Viso JR, Carmona JR, Ruiz G (2008) Shape and size effects on the compressive strength of high-strength concrete. *Cement Concr Res* 38:386–395.
2. Mogi K (1962) The influence of the dimensions of specimens on the fracture strength of rocks. *Bull Earthquake Res Inst* 40:175–185.
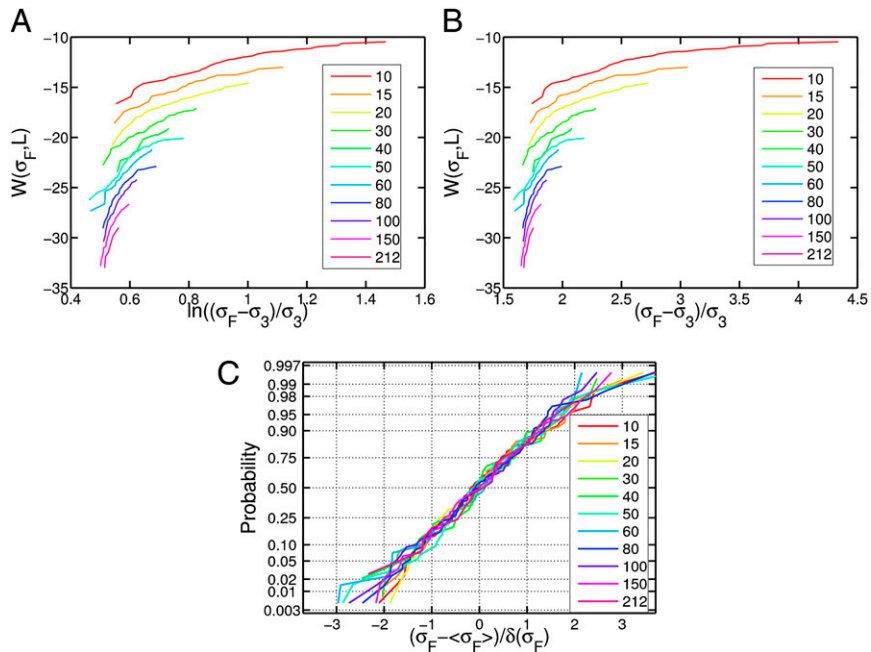
Fig. S2. Distribution of multiaxial compressive strength for the discrete-element model of frictional granular media (LC1 samples; details in *SI Text*). (*A* and *B*) Weibull (*A*) and Gumbel (*B*) statistics, where $W(L, \sigma_f) = \ln(-\ln(1 - P_F(\sigma))/L^2)$ and $P_F(\sigma)$ is the (cumulative) probability of failure under an applied stress σ. Because data obtained for different sample sizes do not collapse onto a single straight line, compressive strengths do not follow either Weibull or Gumbel statistics. (*C*) Normal probability plot for the standard distributions. The collapse onto a single straight line argues for Gaussian statistics.

Table S1. Parameters describing the initial properties of granular samples considered and the finite-size scaling of compressive strength

Sample type	ν_{FS}	A	B	L_A	L_B	σ_∞/σ_3	Φ_{ini}	Z^*_{ini}
HC	1.01	3.36	4.14	1.55	1.92	2.17	0.847 ± 0.001	4
LC1	1.07	2.68	6.32	1.68	4.21	1.65	0.847 ± 0.001	3 ± 0.1
LC2	1.03	2.13	5.52	2.27	6.06	0.96	0.819 ± 0.002	3 ± 0.1